A preliminary experimental investigation of local isotropy in high-Reynolds-number turbulence

By Srinivas V. Veeravalli and Seyed G. Saddoughi

Detailed measurements of the velocity field were made in the wall boundary layer of the 80′ by 120′ facility at NASA Ames. The Reynolds Number R_λ, based on the Taylor microscale λ at the measurement location, was approximately 1450, one of the largest attained in laboratory flows.

The data indicate that to within measurement accuracy, the w-spectrum follows, but the v-spectrum deviates from, the isotropic relation in the inertial subrange. No definite statement can be made regarding local isotropy for the dissipating scales because the spectral measurements were contaminated by high-frequency electrical noise, but it appears that the inertial-subrange anisotropy persist in the dissipation region.

1. Motivation and objectives

1.1. Background

The hypothesis of local isotropy at high Reynolds number proposed by Kolmogorov (1941, 1962) states that the small-scale structures of turbulent motions are independent of large-scale structures and mean deformations. This hypothesis is an integral element of most approaches to understanding turbulence be they theoretical, modeling, or even computational methods like large-eddy simulation.

Local isotropy greatly simplifies the problem of turbulence. The total turbulent energy dissipation ϵ, which in the usual notation is given by

$$\begin{aligned}\epsilon = \nu\Bigg[&2\overline{\left(\frac{\partial u}{\partial x}\right)^2} + \overline{\left(\frac{\partial v}{\partial x}\right)^2} + \overline{\left(\frac{\partial w}{\partial x}\right)^2} + \overline{\left(\frac{\partial u}{\partial y}\right)^2} + 2\overline{\left(\frac{\partial v}{\partial y}\right)^2} + \overline{\left(\frac{\partial w}{\partial y}\right)^2} \\ &+ \overline{\left(\frac{\partial u}{\partial z}\right)^2} + \overline{\left(\frac{\partial v}{\partial z}\right)^2} + 2\overline{\left(\frac{\partial w}{\partial z}\right)^2} \\ &+ 2\overline{\left(\frac{\partial u}{\partial y}\right)\left(\frac{\partial v}{\partial x}\right)} + 2\overline{\left(\frac{\partial u}{\partial z}\right)\left(\frac{\partial w}{\partial x}\right)} + 2\overline{\left(\frac{\partial v}{\partial z}\right)\left(\frac{\partial w}{\partial y}\right)}\Bigg],\end{aligned} \tag{1}$$

reduces to $\epsilon = 15\nu\overline{(\partial u/\partial x)^2}$, in locally isotropic turbulence because the first nine terms in equation (1) are equal to each other and the remaining three terms are each equal to $-\overline{(\partial u/\partial x)^2}$ (see Taylor 1935).

In the high-wavenumber region of the spectrum, Kolmogorov's universal equilibrium hypothesis states that $E_{11}(k_1)/(\varepsilon\nu^5)^{\frac{1}{4}}$ is a universal function of $(k_1\eta)$,

where $\int_0^\infty E_{11}(k_1)\,dk_1 = \overline{u^2}$, k_1 is the longitudinal wavenumber and $\eta = (\nu^3/\varepsilon)^{\frac{1}{4}}$ is the Kolmogorov length scale.

If the motion is isotropic, the transverse spectra $E_{22}(k_1)$ (for the velocity component normal to the wall) and $E_{33}(k_1)$ (for the spanwise component) are uniquely determined from the longitudinal spectrum (Batchelor 1953):

$$E_{22}(k_1) = E_{33}(k_1) = \frac{1}{2}(1 - k_1\frac{\partial}{\partial k_1})E_{11}(k_1). \tag{2}$$

In the inertial subrange, the 3D spectrum takes the form (Kolmogorov 1941)

$$E(k) = C_1\varepsilon^{2/3}k^{-5/3}, \tag{3}$$

where k is the wavenumber magnitude, and, assuming isotropy, the one-dimensional longitudinal and transverse spectra are

$$E_{11}(k_1) = C_2\varepsilon^{2/3}k_1^{-5/3} \tag{4}$$

and

$$E_{22}(k_1) = E_{33}(k_1) = C_2'\varepsilon^{2/3}k_1^{-5/3} \tag{5}$$

respectively. The constant C_1 is equal to $\frac{55}{18}C_2$, and equation (2) evaluated in the inertial subrange gives $C_2'/C_2 = 4/3$.

1.2. Previous work

There have been many experiments, conducted in wakes, jets, mixing layers, a tidal channel, and atmospheric and laboratory boundary layers, in which the concept of local isotropy has been investigated. One of the earliest studies was by Townsend (1948), who took measurements in the wake of a cylinder and verified local isotropy. Browne, Antonia & Shah (1987) took a comprehensive set of measurements in the wake of a cylinder at low R_λ ($\approx$ 40 to 80) and found that local isotropy was not satisfied in the dissipation range. Townsend (1954) concluded from later measurements that when a uniform mean rate of strain was imposed on isotropic turbulence, the dissipating eddies were not isotropic. The recent data taken by Karyakin, Kuznetsov & Praskovsky (1991) in a return channel at $R_\lambda \approx 3000$ indicates that neither the inertial nor dissipation ranges are isotropic. However, Mestayer (1982), who examined this question in a boundary layer at $R_\lambda \approx 600$, concluded that local isotropy was satisfied by the dissipating eddies but not in the inertial subrange. Some additional experiments are listed in Figure 11.

There have recently been a number of theoretical and computational studies stressing the importance of *non-local* (in Fourier space) interactions in the energy cascade process, and this brings into question Kolmogorov's concept of a self-similar cascade. Domaradzki & Rogallo (1988) and Domaradzki, Rogallo & Wray (1990) showed that the energy transfer between similar small scales is largest when the third leg of the triad is a large scale. Yeung & Brasseur (1991) also demonstrated the importance of non-local transfer in their numerical simulations and argued that

such interactions are important even in the high-Reynolds-number limit. However, Waleffe (1991) shows that if one considers all possible non-local triads, the net local transfer due to non-local interactions is not significant, thus local isotropy may not be affected by large-scale anisotropy or strain. Durbin & Speziale (1991) examined the equation for the dissipation rate tensor, ϵ_{ij}, and showed that local isotropy is inconsistent with the presence of mean strain.

From the foregoing brief review (for a more comprehensive one see Van Atta 1991), it is clear that there is no consensus regarding the local-isotropy hypothesis, and, therefore, it seems worthwhile to undertake a fresh experimental investigation into this question.

2. Accomplishments

2.1. Apparatus and measurement techniques

The experiments described here were conducted in the boundary layer on the test-section ceiling of the full scale aerodynamics facility at NASA Ames. The test section is 80′ high, 120′ wide, and approximately 155′ long. All four walls of the test section are lined with acoustic paneling, yielding a rough-wall boundary layer. The measurement station was located towards the end of the test section on the centerline of the tunnel. These experiments were conducted while NASA engineers were investigating the flow around an F-18 fighter aircraft in the central region of the working section.

Mean-flow, broadband-turbulence and spectral measurements were taken at two nominal freestream velocities (U_e) of 40 and 50 m/s.

The hot-wire instrumentation used consisted of Dantec model P51 cross-wire probes, modified to support 2.5 μm Platinum plated Tungsten wires with an etched length of approximately 0.6 mm, TSI model 1050 hot-wire bridges, and model 1052 signal conditioners. The X-wires were oriented nominally at $\pm 45°$ to the mean-flow direction. All of the hot-wires were operated with an overheat ratio of 1.8. The square-wave response of the anemometers was adjusted for optimum damping, and their frequency response was better than 100 kHz.

The hot-wire output voltages were digitized on a micro computer equipped with an Adtek AD830 12-bit analog-to-digital converter. The analog signals for the broadband-turbulence measurements were low-pass filtered (Rockland model 452 and 852 units) at 70 kHz. In order to span the full frequency extent of the spectra with a modest amount of disk storage space, the data were obtained in three spectral bands using a band-pass filtering technique with approximately one decade of overlap (in frequency) between neighboring bands. This also permitted us to change the dynamic range of the analog-to-digital converter to match that expected in a given band. Overall, the resulting frequency bandwidth for spectra was 0.5 Hz to 100 kHz.

For each point in a turbulence profile, 50 records of 1024 samples were taken. Sampling frequencies varied from 1000 Hz near the wall to 600 Hz near the edge of the boundary layer. For spectral measurements, 200 records of 4096 samples each were recorded in the low frequency band and 400 records in the higher frequency

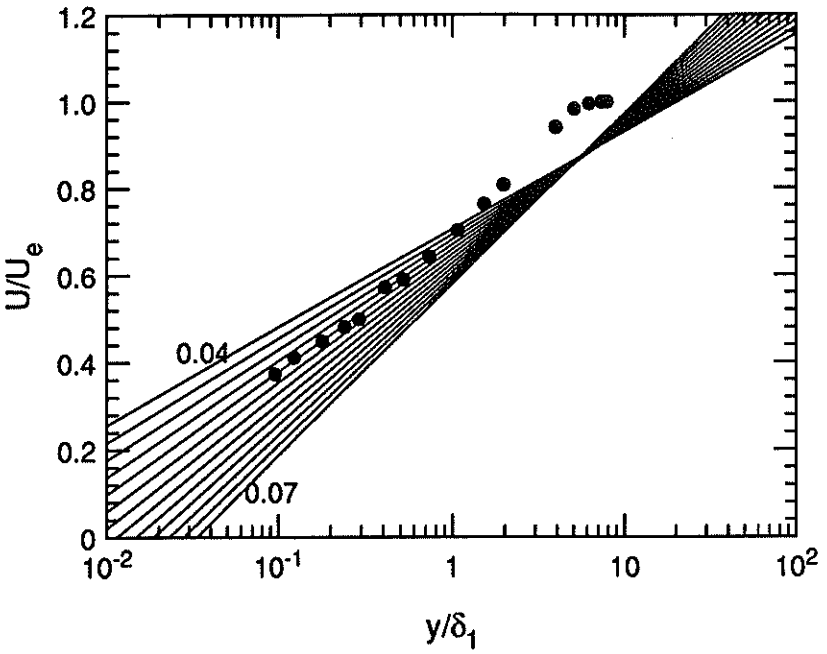

FIGURE 1. Mean-velocity profile ($U_e \approx 35m/s$). 'Modified Clauser chart' method for rough-wall boundary layers (Perry & Li 1990). δ_1 is the displacement thickness, and each of the straight lines corresponds to a constant value of $(C_f/2)^{1/2}$. Error in origin, $e = 1mm$.

bands. In each case, the sampling frequency was three to four times larger than the low-pass filter cut-off frequency in order to avoid aliasing errors. The spectral densities of the hot-wire signals were computed by a fast-Fourier-transform algorithm. To convert frequencies to wavenumbers, Taylor's hypothesis was used.

2.2. Results and discussion

2.2.1. Mean flow and broadband turbulence

The overall features of the boundary layer were measured in detail to verify that the flow followed standard behavior and that the interference from the F-18 aircraft was not significant. These results facilitated the choice of points at which spectral measurements were taken.

One of the problems in rough-wall boundary-layer experiments is to measure the local skin-friction coefficient, C_f, accurately because, in addition to C_f, there are two other unknown variables which have to be determined. These are the roughness function and the error in origin, e (Perry & Joubert 1963). The latter variable is the distance below the crests of the roughness elements which defines an origin for the profiles that will give the logarithmic distribution of velocity near the wall. Perry & Li (1990) have developed a modified Clauser plot to find e that is based on the original method of Perry & Joubert. This method was used to analyze the mean-velocity data, and as an example, a profile taken at $U_e \approx 35m/s$ is shown in Figure

1. The profile shape appears to be typical and $e \approx 1mm$. The C_f value obtained for this case was about 0.005.

The normalized profiles of the Reynolds normal stresses ($\overline{u^2}/U_e^2, \overline{v^2}/U_e^2, \overline{w^2}/U_e^2$) and the shear stress, $-\overline{uv}/U_e^2$, at $U_e \approx 50m/s$, are shown in Figures 2 and 3 respectively.

The agreement between $\overline{u^2}/U_e^2$ data obtained by the uv and uw X-wires is very good. In the outer part of the boundary layer, these profiles have the standard shapes, but near the wall there appears to be a sharp rise in the values of all the stresses. In Figure 3 the repeatability of this phenomenon is illustrated. We will not attempt to explain this anomalous behavior, but it may be noted that it could have resulted from the acoustic panels. To verify that the outer part of the present boundary layer did follow the standard behavior, a Reynolds-shear-stress profile is compared in Figure 4 with the profiles of Perry & Li taken over a d-type rough wall at various Reynolds numbers. In this figure, δ_H is the Hama boundary-layer thickness, which is equal to $(U_e\delta_1)/(CU_\tau)$, where $C = 3.3715$ and the friction velocity, U_τ, was obtained from the modified Clauser chart. Clearly, there is a good agreement between these two sets of data in the outer part of the layer.

A profile of the structural parameter $a_1 = -\overline{uv}/q^2$, where q^2 $(= \overline{u^2} + \overline{v^2} + \overline{w^2})$ is twice the turbulent kinetic energy, is plotted in Figure 5. In the canonical flat-plate boundary layer, this parameter is about 0.15, except near the surface and the outer edge. The fairly constant value of about 0.13 obtained in the present experiment indicates that the turbulence structure of the boundary layer was not significantly affected by any undesirable perturbation. In local equilibrium (dissipation = production), the mean strain rate parameter, Sq^2/ε, becomes equal to $1/a_1$, where $S = \partial U/\partial y$. For the present case $Sq^2/\varepsilon \approx 8$.

Once we verified that the outer part of the boundary layer followed the standard behavior, the next step was to choose the location y/δ for detailed spectral measurements. Figure 6 shows the profiles of rms longitudinal velocity fluctuations, normalized by the local mean velocity, taken at different freestream velocities and with different wires. This plot not only shows the good repeatability of the results but also indicates that spectral measurements have to be taken for $y/\delta \geq 0.25$ in order to satisfy Lumley's (1965) criterion (that errors arising from the use of Taylor's hypothesis will be small if $\sqrt{\overline{u^2}}/U < 0.10$).

Figure 7 shows a profile of R_λ $(\equiv \sqrt{\overline{u^2}}\lambda/\nu)$, where $\lambda \equiv \sqrt{\overline{u^2}/\overline{(\partial u/\partial x)^2}}$ and the measured values of Reynolds stresses were used in conjunction with the assumption that $\varepsilon = -\overline{uv}\partial U/\partial y = 15\nu\overline{(\partial u/\partial x)^2}$. The maximum R_λ occurs at $y/\delta \approx 0.5$.

2.2.2. Spectra

Based on the results presented in the previous sections, the point $y/\delta \approx 0.4$ was chosen for the spectral measurements. This location in the boundary layer has the following advantages: (a) it is well inside the layer and boundary-layer edge intermittency effects are not present; (b) it is well away from the wall, so that the 'bump' in the Reynolds stresses is avoided; (c) it is in the region where Taylor's hypothesis can be used within the accepted accuracy, and (d) it is the point of

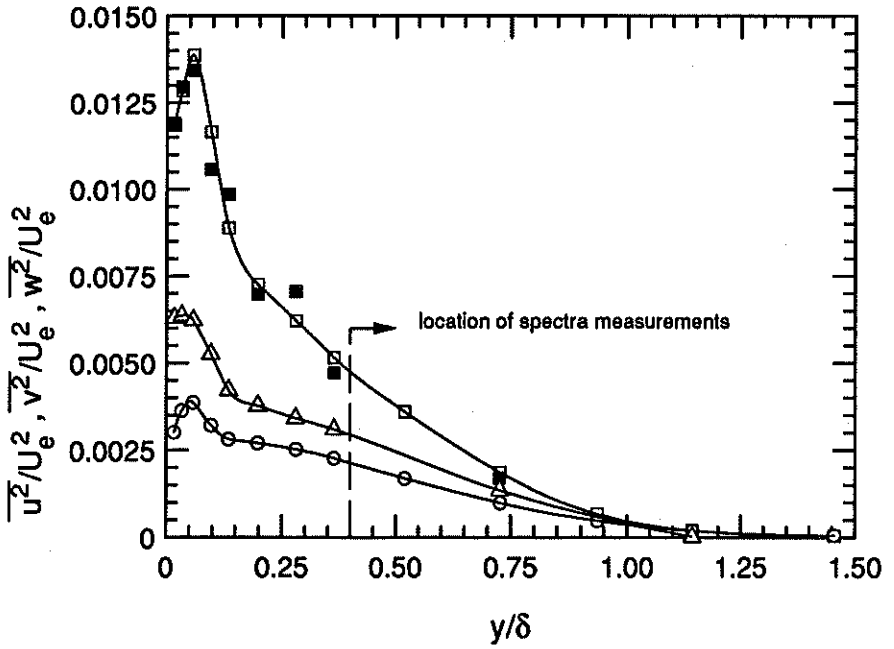

FIGURE 2. Profiles of Reynolds normal stresses ($U_e \approx 50m/s$). □ , $\overline{u^2}/{U_e}^2$ (from uv X-wire); ■ , $\overline{u^2}/{U_e}^2$ (from uw X-wire); ○ , $\overline{v^2}/{U_e}^2$; △ , $\overline{w^2}/{U_e}^2$.

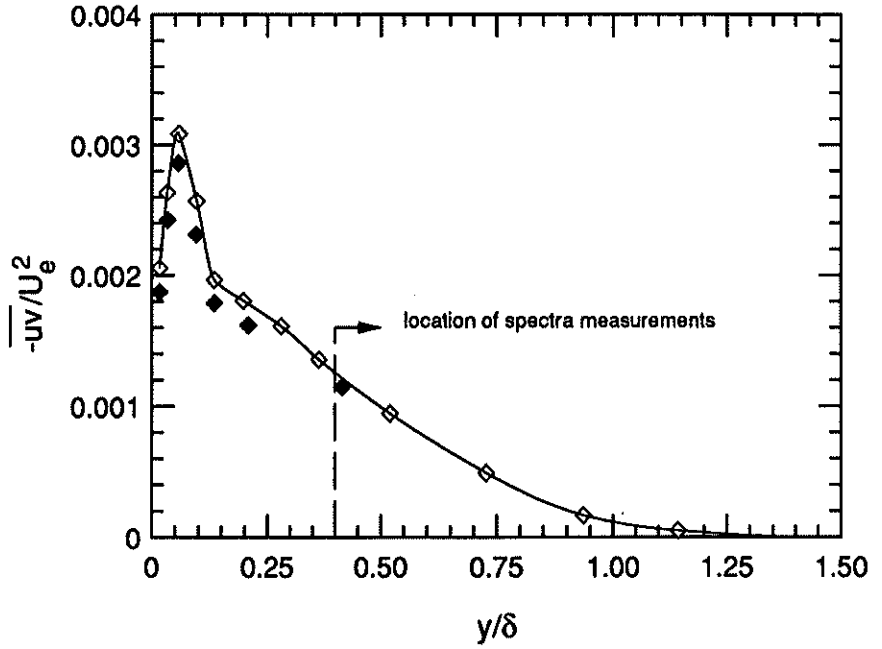

FIGURE 3. Profiles of Reynolds shear stresses taken on different days but at the same freestream velocity ($U_e \approx 50m/s$).

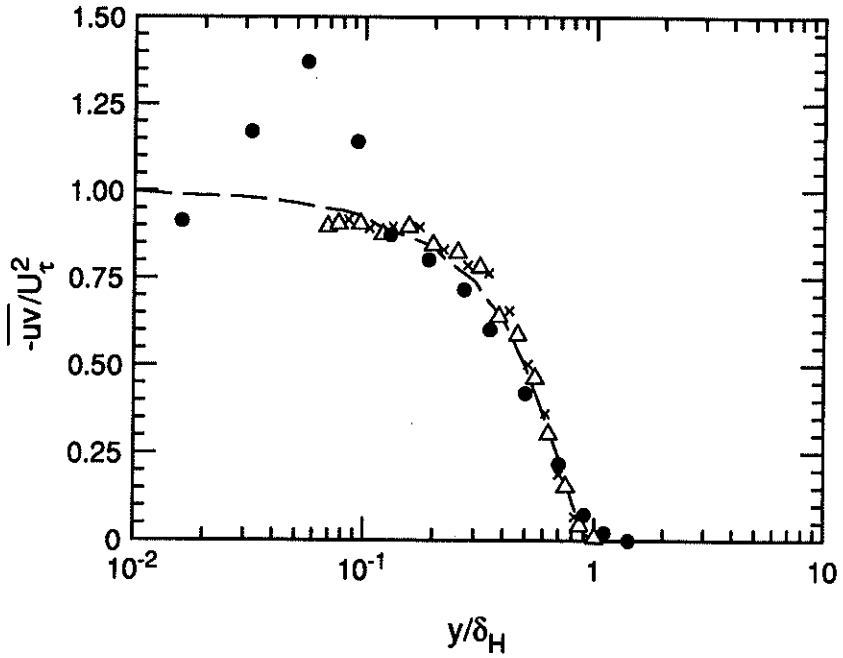

FIGURE 4. Comparison of the present $-\overline{uv}/U_\tau^2$ profile ($\bullet$) for $R_\theta \approx 300000$ with those of Perry & Li (1990) ($\times$ and $\triangle$ for low R_θ and ---- for $R_\theta \to \infty$).

maximum R_λ. Flow parameters for spectral measurements are given in Table 1.

The freestream velocity, U_e (m/s)	≈ 40
The boundary layer thickness, δ (m)	≈ 1.0
The momentum thickness Reynolds number, R_θ	$\approx 300{,}000$
Measurement location, y/δ	≈ 0.4
Local mean velocity, U (m/s)	$= 35.1$
Local turbulence intensity, $\sqrt{\overline{u^2}}/U$	$= 0.08$
Microscale Reynolds number, R_λ	≈ 1450
Kolmogorov length scale, η (mm)	≈ 0.1
Ratio of X-wire span, $l/\sqrt{2}$ to η	≈ 4.3

TABLE 1: Flow Parameters.

Figure 8 shows $E_{11}(k_1)$ obtained in the three measurement bands. Clearly, the agreement between the three segments of the spectrum is very good. The collapse for the transverse spectra was equally good. The spectrum spans five decades in wavenumber and eight decades in amplitude and has a $-5/3$ slope over a region spanning approximately two decades in wavenumber. This is one of the longest $-5/3$ ranges seen in laboratory flows. It must be noted that although the measurements extend up to $k_1\eta \approx 1$, the data are reliable only up to $k_1\eta \approx 0.3$ because the

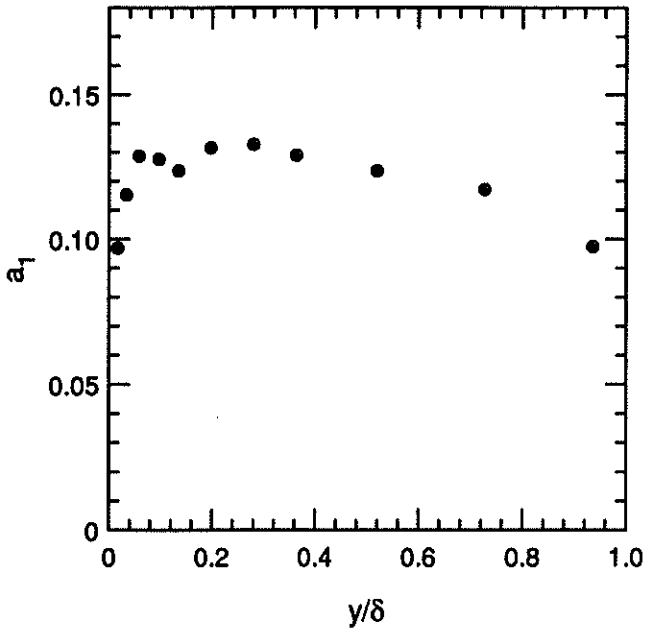

FIGURE 5. Profile of structure parameter a_1 ($U_e \approx 50m/s$).

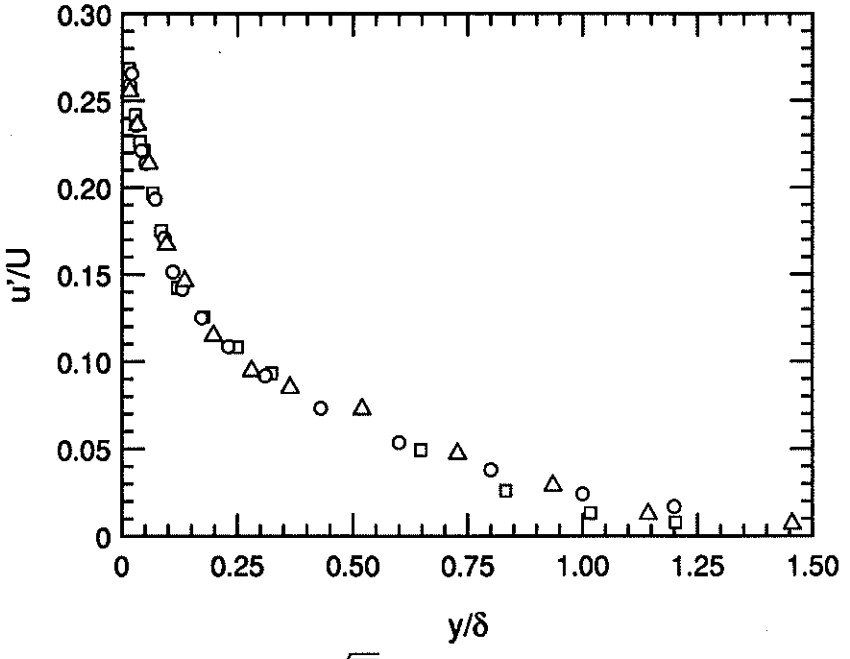

FIGURE 6. Comparison of $\sqrt{u^2}/U$ profiles taken with different wires. □ , $5\mu m$ single wire at $U_e \approx 35m/s$; ○ , $5\mu m$ single wire at $U_e \approx 50m/s$; △ ,$2.5\mu m$ uv X-wire at $U_e \approx 50m/s$.

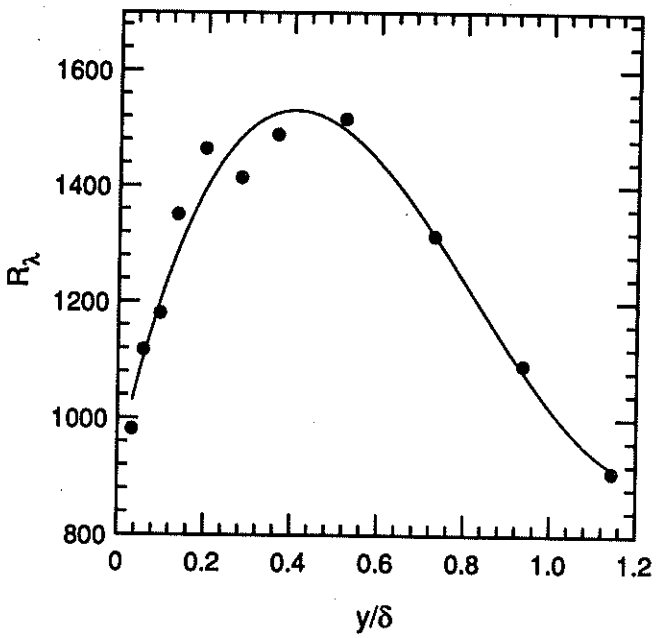

FIGURE 7. Profile of Reynolds number based on Taylor's micro-scale, λ ($U_e \approx 50m/s$).

combined error in the spectrum, due to lack of sufficient spatial resolution (Wyngaard 1968) and electronic noise, exceeds 20% for $k_1\eta > 0.3$. To illustrate the latter effect, u- and w-spectra for the third band-pass segment are shown in Figure 9. The presence of noise and the effect of filter cut-off at high wavenumbers are quite evident. To rectify this situation, it was assumed that the spectrum taken at $y/\delta \approx 1.4$ corresponded to pure noise (including the wind-tunnel turbulence which resides mainly at very low wavenumbers), and this spectrum was subtracted from the one taken at $y/\delta \approx 0.4$. As shown in Figure 10, this process resulted in a spectrum which dropped off smoothly at the high-wavenumber end. Nevertheless, no definite conclusions will be made for the region $k_1\eta > 0.3$. Figure 11 shows a comparison between the present data and a compilation of some experimental work taken from Chapman (1979) with later additions. The agreement is very good. Note that the behavior of the return-channel data of Karyakin *et al.* (1991) at low-wavenumbers perhaps indicates the presence of large-scale unsteadiness in their flow.

To investigate the isotropy of the inertial subrange, we use equations (4) and (5) and present in Figure 12 the compensated spectra $k_1^{-5/3}E_{ii}(k_1)$, where $i = 1, 2$ or 3 corresponds to u, v or w respectively. In the inertial subrange, these compensated spectra should be independent of wavenumber, and the v- and w-spectra should be equal to each other and larger than the u-spectrum by a factor 4/3. Also shown in Figure 12(a) are the seventh-order least-square polynomial fits to the u-spectra obtained from the uw and uv X-wires. These u-spectra are in good agreement,

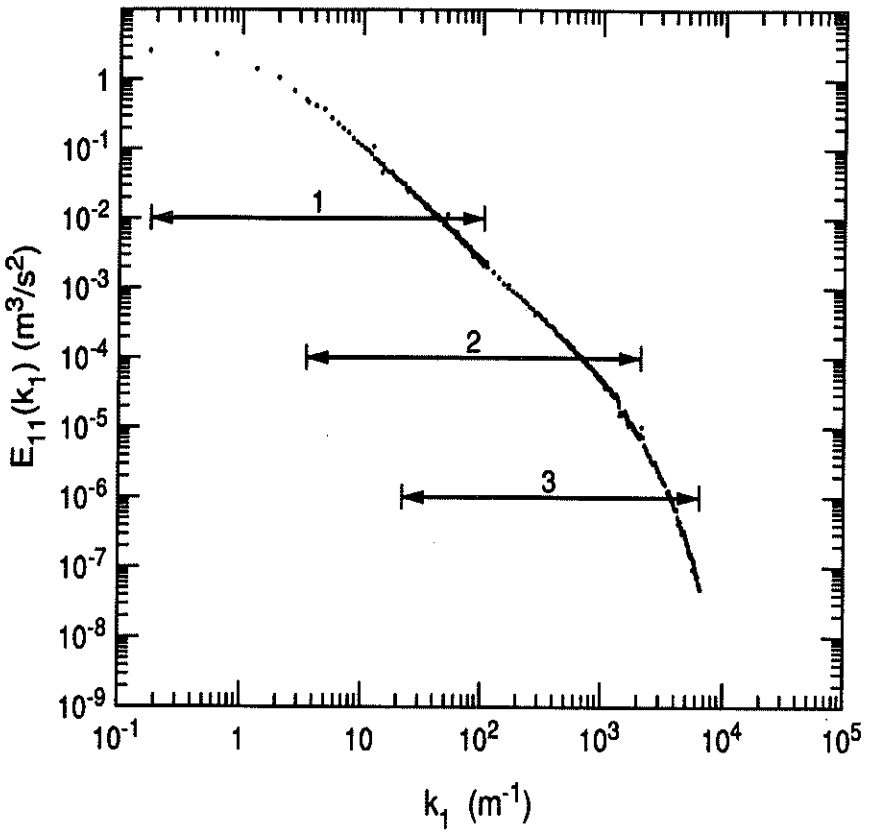

FIGURE 8. Longitudinal power spectrum, $E_{11}(k_1)$. The numbered arrows indicate the three spectral bands chosen.

giving some indication that the differences between v- and w-spectra (figure 12b and 12c) in the inertial-subrange region may be real. Taking the dissipation as $\varepsilon = 15\nu \int k_1^2 E_{11}(k_1) dk_1$, $C_2 \approx 0.58$ and $C_2' \approx 0.75$ were obtained from u- and w-spectra respectively. These both yield $C_1 \approx 1.75$. Therefore, it appears that w-spectrum follows, but the v-spectrum deviates from, the isotropic relation in the inertial subrange.

The spectral distribution of the ratio of the measured w-spectrum to v-spectrum, $E_{33}^{meas}(k_1)/E_{22}^{meas}(k_1)$, in the inertial and the dissipation ranges is shown in Figure 13. For isotropic turbulence, this ratio should be equal to 1. In the $-5/3$ region, $10^{-3} < k_1\eta < 10^{-1}$, the average value of this ratio is about 1.43. Also, it appears that the inertial-subrange anisotropy persists in the dissipation range; however, as mentioned above, the data are not reliable for $k_1\eta > 0.3$.

Undoubtedly, the present study (see also Veeravalli, Saddoughi, Praskovsky & Bradshaw 1991) indicates that further experiments, which encompass large sets of measurement points in a variety of flows, are needed to resolve the unanswered issues.

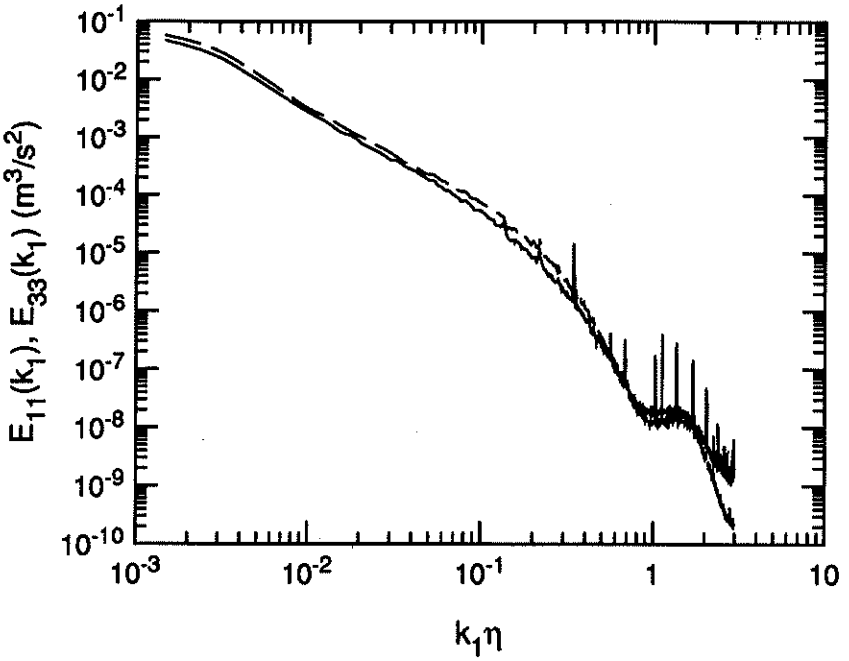

FIGURE 9. u (——) and w (- - - -) spectra at $y/\delta \approx 0.4$ for the third bandpass region.

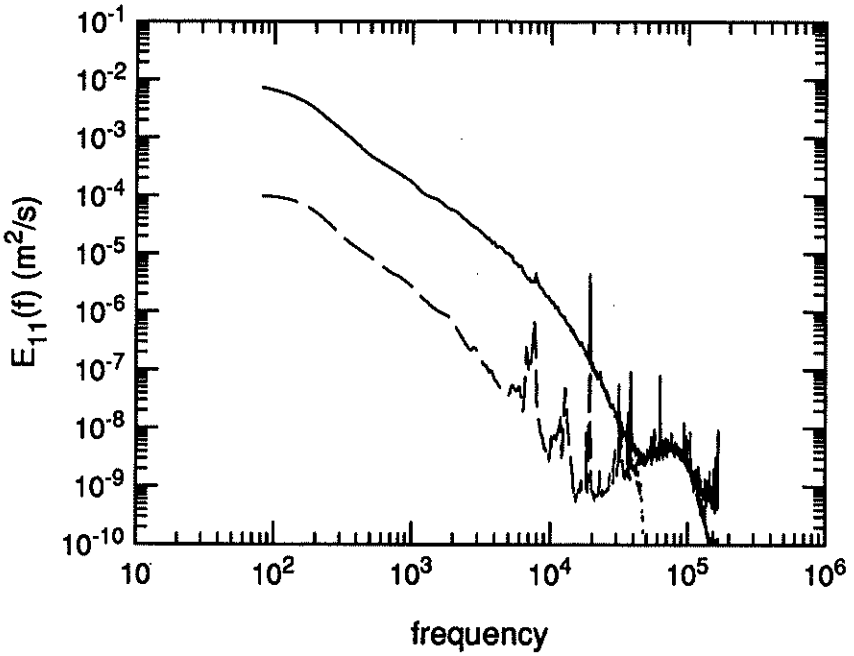

FIGURE 10. Noise subtraction. —— , noisy spectrum at $y/\delta \approx 0.4$; - - - - , noise spectrum at $y/\delta \approx 1.4$; ····· , noiseless spectrum at $y/\delta \approx 0.4$.

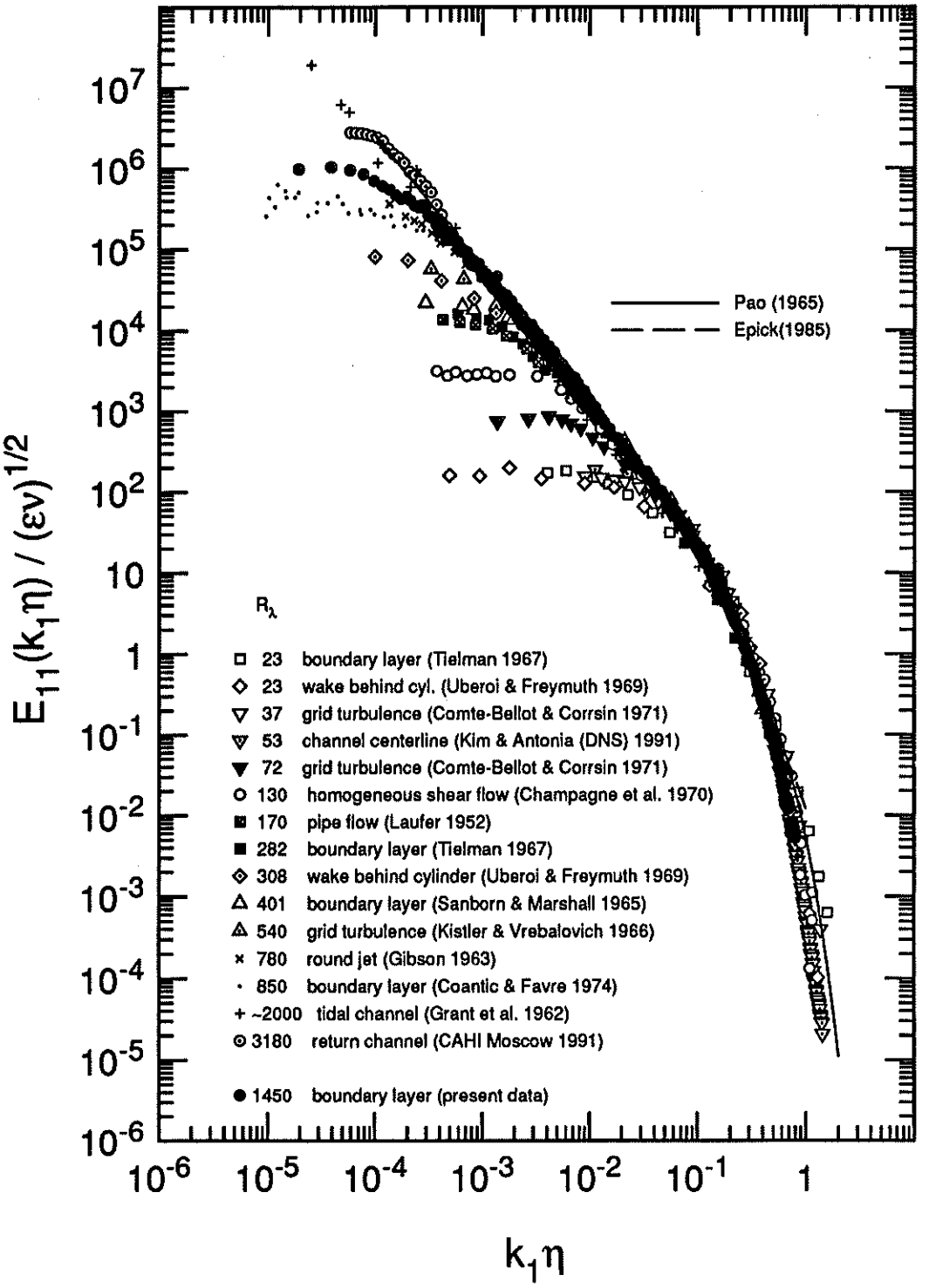

FIGURE 11. Normalized longitudinal spectrum compared with data from other experiments. This compilation is from Chapman (1979) with later additions.

3. Future plans

As explained above, the present measurements were contaminated by high frequency electrical noise, which prevented accurate determination of local isotropy in the dissipating scales. We plan to concentrate on reducing the noise in the next phase of the measurements.

Apart from obtaining a new set of instruments which have much lower background noise, it may be possible to avoid the high-frequency noise by repeating the measurements for the same x location but at lower freestream velocities.

It is known that for a self-preserving boundary layer, at a given y/δ position

$$\epsilon \sim U_\tau^3/\delta. \tag{6}$$

As a first estimate, if one uses power-law approximations for boundary-layer thickness and local skin-friction coefficient for a smooth flat plate (see e.g. Schlichting 1979), it can be shown easily that, at a given x, dissipation scales with free-stream velocity as

$$\epsilon \sim (U_e)^{29/10}. \tag{7}$$

This in turn implies that the Kolmogorov length scale, η, and frequency, f_η, at that location vary with U_e as

$$\eta \sim (U_e)^{-29/40}, \tag{8}$$

and

$$f_\eta \sim (U_e)^{69/40}. \tag{9}$$

Also, using the isotropic relation to calculate λ, it is seen that

$$R_\lambda \sim (U_e)^{7/20}. \tag{10}$$

Furthermore, at the high-wavenumber end of the spectrum, if Kolmogorov scaling is applied at $k_1\eta = 1$, then

$$E_{11}(k_1\eta) \sim v^2, \tag{11}$$

where $v = (\nu\epsilon)^{1/4}$ is the Kolmogorov velocity scale. The energy spectrum at the Kolmogorov frequency will then scale as

$$E_{11}(f_\eta) \sim (U_e)^{-11/40}, \tag{12}$$

which indicates that the energy content of the tail of the spectrum increases with reduction in freestream velocity.

Therefore, at the same measurement station at which high speed data were taken in the boundary layer in the 80′ by 120′ wind tunnel, based on the above relationships, the values in Table 2 can be obtained for $y/\delta \approx 0.4$ at lower speeds:

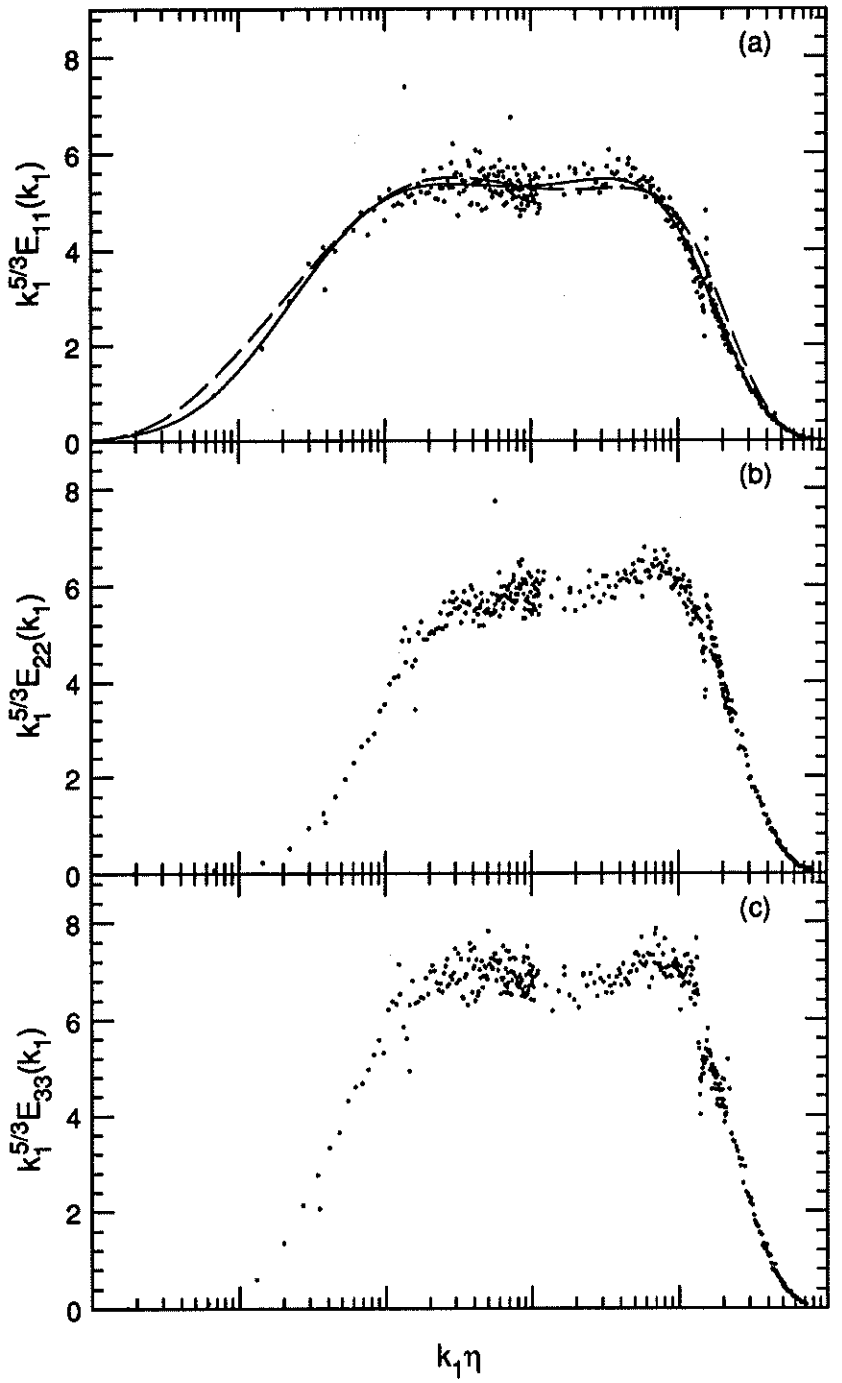

FIGURE 12. Compensated longitudinal and transverse spectra (symbols show the unsmoothen data). (a) u-spectra (• , unsmoothen data from uv X-wire; ——— , polynomial fit to data from uv X-wire; ---- , polynomial fit to data from uw X-wire). (b) v-spectrum; (c) w-spectrum.

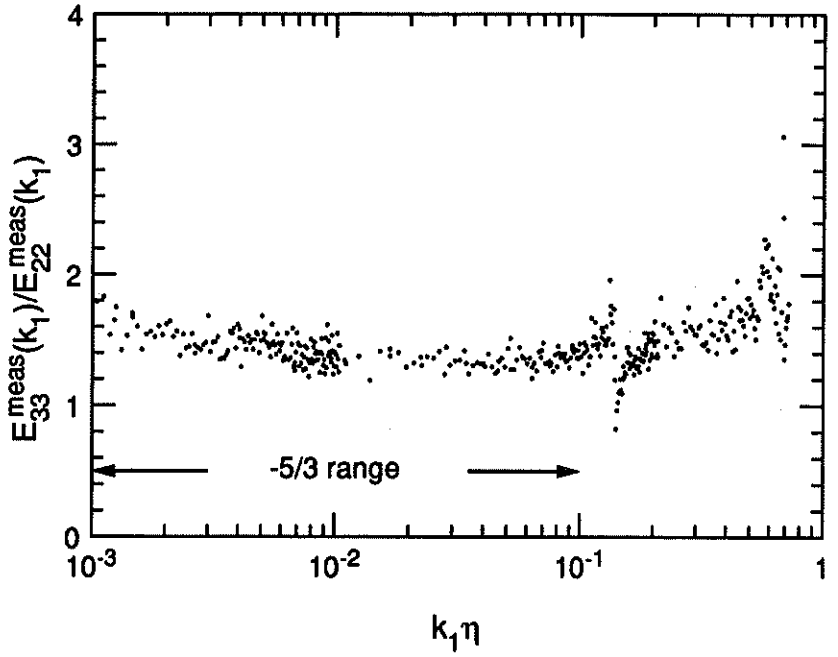

FIGURE 13. Spectral distribution of the ratio of the measured w-spectrum to v-spectrum.

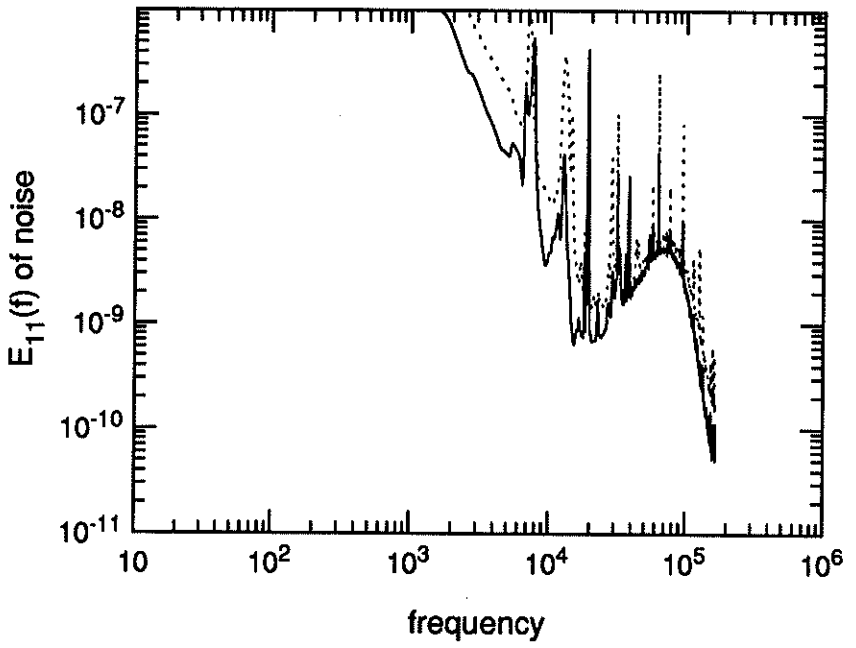

FIGURE 14. Noise spectra at two different freestream velocities. ——— , $U_e \approx 40m/s$; - - - - , $50m/s$.

	U_e (m/s)	η (mm)	f_η (Hz)	R_λ	$(l/\sqrt{2})/\eta$	u_{ratio}	v_{ratio}
measured	40	0.10	56,000	1,450	4.5	0.45	0.25
expected	20	0.165	17,000	1,100	2.6	0.90	0.55
expected	10	0.27	5,100	900	1.7	0.97	0.80

TABLE 2: Flow parameters at various freestream velocities. $u_{ratio} \equiv E^m_{11}/E^t_{11}$ and $v_{ratio} \equiv E^m_{22}/E^t_{22}$ at $k_1\eta = 1$, where E^m_{ii} and E^t_{ii} are the measured and true spectra respectively: from Wyngaard (1968). These ratios will be equal to 1, if there are no spatial-resolution errors in the hot-wire measurements.

Figure 14 shows the noise spectra taken at two different freestream velocities. The part of the spectrum dominated by noise has a slope of 2 and is (roughly) independent of velocity since its origins are electrical.

The overall implication of the above analysis is that with a four-fold reduction in the freestream velocity, one can reduce the Kolmogorov frequency by a factor of 10, more than double the spatial resolution of the hot-wires, increase the energy content in the tail of the spectrum by about 50%, and avoid the noise to a large extent, without much sacrifice in R_λ. It is hoped that the continuation of experiments in the 80′ by 120′ wind tunnel will produce an internally consistent set of results, which will lead to more definite conclusions regarding the local-isotropy hypothesis.

Acknowledgements

We wish to thank the Full-Scale Aerodynamics Research Division at NASA Ames for permitting us to use their facility, and to thank the F-18 test team, especially Dr. J. Ross and P. Zell, for their cooperation during the experiments.

Dr. A. A. Praskovsky from the Central Aero-Hydrodynamic Inst., Moscow, helped us analyze the data, and Prof. P. Bradshaw guided us throughout this project. We thank them both for all their help and advice, without which this work would have not been possible. We also wish to thank Prof. P. Moin, Prof. W. C. Reynolds, Dr. J. Kim, and Dr. R. S. Rogallo for their encouragement and for valuable discussions during the course of this project.

REFERENCES

BATCHELOR, G. K., 1953 *The Theory of Homogeneous Turbulence.* Cambridge University Press.

BROWNE, R. A., ANTONIA, A. A. & SHAH, D. A., 1987 Turbulent energy dissipation in a wake. *J. Fluid Mech.* **179,** 307-326.

CHAPMAN, D., 1979 Computational aerodynamics development and outlook. *AIAA J.* **17,** 1293.

DOMARADZKI, A. J., & ROGALLO, R. S., 1988 Energy transfer in isotropic turbulence at low Reynolds numbers. *Proc. Summer Program, Center for Turbulence Research.* **CTR-S88,** Center for Turbulence Research, Stanford University/NASA Ames. 169-177.

DOMARADZKI, A. J., ROGALLO, R. S., & WRAY, A. A., 1990 Interscale energy transfer in numerically simulated homogeneous turbulence. *Proc. Summer Program, Center for Turbulence Research, Stanford Univ.* **CTR-S90,** Center for Turbulence Research, Stanford University/NASA Ames. 319-329.

DURBIN, P. A. & SPEZIALE, C. G., 1991 Local anisotropy in strained turbulence at high Reynolds numbers. *Recent Advances in Mechanics of Structured Continua.* **117,** 29-32.

KARYAKIN, M. Y., KUZNETSOV, V. R. & PRASKOVSKY, A. A., 1991 *Izv. AN SSSR, Mech. Zhidk. i Gaza,* **5.**

KIM, J. & ANTONIA, R. A., 1991 Isotropy of small-scale turbulence at low Reynolds number. *Submitted to J. Fluid Mech.*

KOLMOGOROV, A. N., 1941 The local structure of turbulence in incompressible viscous fluid for very large Reynolds numbers. *C. R. Acad. Sci U.R.S.S.* **30,** 301.

KOLMOGOROV, A. N., 1962 A refinement of previous hypotheses concerning the local structure of turbulence in a viscous incompressible fluid at high Reynolds number. *J. Fluid Mech.* **13,** 82-85.

LUMLEY, J. L., 1965 Interpretation of time spectra measured in high-intensity shear flows. *Phys. Fluids.* **8,** 1056-1062.

MESTAYER, P., 1982 Local isotropy and anisotropy in a high-Reynolds-number turbulent boundary layer. *J. Fluid Mech.* **125,** 475-503.

PERRY, A. E. & JOUBERT, P. N., 1963 Rough wall boundary layers in adverse pressure gradients. *J. Fluid Mech.* **17,** 193-211.

PERRY, A. E. & LI, J. D., 1990 Experimental support for the attached-eddy hypothesis in zero-pressure-gradient turbulent boundary layers. *J. Fluid Mech.* **218,** 405-438.

SCHLICHTING, H., 1979 *Boundary Layer Theory.* McGraw-Hill.

TAYLOR, G. I., 1935 Statistical theory of turbulence. *Proc. Roy. Soc. Lond. A.* **151,** 421-478.

TOWNSEND, A. A., 1948 Local isotropy in the turbulent wake of a cylinder. *Austral. J. Sci. Res.* **2,** 161-174.

TOWNSEND, A. A., 1954 The uniform distortion of homogeneous turbulence. *Q. J. Mech. Appl. Math.* **7,** 104-127.

VAN ATTA, C., 1991 Local isotropy of the smallest scales of turbulent scalar and velocity fields. *Proc. Roy. Soc. Lond. A.* **434,** 139-147.

VEERAVALLI, S. V., SADDOUGHI, S. G., PRASKOVSKY, A. A. & BRADSHAW, P., 1991 A note on local isotropy in high-Reynolds-number turbulence. *To appear in the Proc. Monte Verita Colloquium on Turbulence, Sept. 9-11, Switzerland.*

WALEFFE, F., 1991 The nature of triad interactions in homogeneous turbulence. *Submitted to Phys. of Fluids A.*

WYNGAARD, J. C., 1968 Measurements of small-scale turbulence structure with hot wires. *J. Sci. Instrum.*, **1**, 1105-1108.

YEUNG, P. K. & BRASSEUR, J. G., 1991 The response of isotropic turbulence to isotropic and anisotropic forcing at the large scales. *Phys. of Fluids A.* **3**, 884-897.